Hearing Research 360 (2018) 31–39

Contents lists available at ScienceDirect

Hearing Research

journal homepage: www.elsevier.com/locate/heares

Research Paper

An operating principle of the turtle utricle to detect wide dynamic range

Jong-Hoon Nam [a, b, *]

[a] Department of Mechanical Engineering, University of Rochester, Rochester, NY, USA
[b] Department of Biomedical Engineering, University of Rochester, Rochester, NY, USA

ARTICLE INFO

Article history:
Received 20 July 2017
Received in revised form
10 September 2017
Accepted 27 September 2017
Available online 9 October 2017

Keywords:
Utricle
Striola
Hair cell
Mechano-transduction

ABSTRACT

The utricle encodes both static information such as head orientation, and dynamic information such as vibrations. It is not well understood how the utricle can encode both static and dynamic information for a wide dynamic range (from <0.05 to >2 times the gravitational acceleration; from DC to > 1000 Hz vibrations). Using computational models of the hair cells in the turtle utricle, this study presents an explanation on how the turtle utricle encodes stimulations over such a wide dynamic range. Two hair bundles were modeled using the finite element method—one representing the striolar hair cell (Cell S), and the other representing the medial extrastriolar hair cell (Cell E). A mechano-transduction (MET) channel model was incorporated to compute MET current (i_{MET}) due to hair bundle deflection. A macro-mechanical model of the utricle was used to compute otoconial motions from head accelerations (a_{Head}). According to known anatomical data, Cell E has a long kinocilium that is embedded into the stiff otoconial layer. Unlike Cell E, the hair bundle of Cell S falls short of the otoconial layer. Considering such difference in the mechanical connectivity between the hair cell bundle and the otoconial layer, three cases were simulated: Cell E displacement-clamped, Cell S viscously-coupled, and Cell S displacement-clamped. Head accelerations at different amplitude levels and different frequencies were simulated for the three cases. When a realistic head motion was simulated, Cell E was responsive to head orientation, while the viscously-coupled Cell S was responsive to fast head motion imitating the feeding strike of a turtle.

1. Introduction

The utricle is one of the inner ear sensory organs that is responsible for sensing the orientation and motion of head (Rabbitt et al., 2004). Together with the saccule, the utricle is called the otolith organ because of the otoconial layer lying on top of the hair cells' stereocilia bundles (hair bundles). The hair cells have polarity: they are most sensitive along the direction of the hair bundle's height gradient (Hudspeth and Corey, 1977; Nam et al., 2007a,b). There exists a conceptual line on the macular surface across which the hair cells' polarity is reversed (the solid curve in Fig. 1). The hair cells in the vicinity along the line of polarity reversal look different from others, and this region is called the striolar region (the shaded area in Fig. 1A, (Fernandez et al., 1990)). Each hair bundle consists of a few dozen stereocilia and one kinocilium. In the striolar region, the kinocilium has similar height with the tallest row of stereocilia, and the stereocilia height gradient is steep (slope angle > 60°). In contrast, in the extrastriolar region, the kinocilium is often several times taller than the rest of the bundle, and the stereocilia height gradient is gentle (<40°). Considering that this variation in hair bundle shapes are correlated with the type of afferent nerves attached to the hair cells (Xue and Peterson, 2006; Li et al., 2008), it is plausible that the hair bundle shapes systematically varying across the macular surface might implicate their functional roles.

A notable difference between the striolar and the extrastriolar hair bundles is their structural connectivity to the otoconial layer (the circles with broken lines, Fig. 1B). The height ratio between the kinocilium and the tallest stereocilia is > 2 for typical medial extrastriolar hair bundle, but the ratio is about 1 for typical striolar hair bundles (Xue and Peterson, 2006). The tall kinocilium of an extrastriolar hair cell (Cell E) is firmly plugged into the otoconial gel. In contrast, the tallest edge of the striolar hair cell bundle (Cell S bundle) falls short of the firm otoconial layer. Presumably, the hair

Abbreviations: MET, Mechano-transduction; FE, finite element

* 212 Hopeman Bldg, Rochester, NY 14627-0132, USA.
E-mail address: jong-hoon.nam@rochester.edu.

https://doi.org/10.1016/j.heares.2017.09.015
0378-5955/

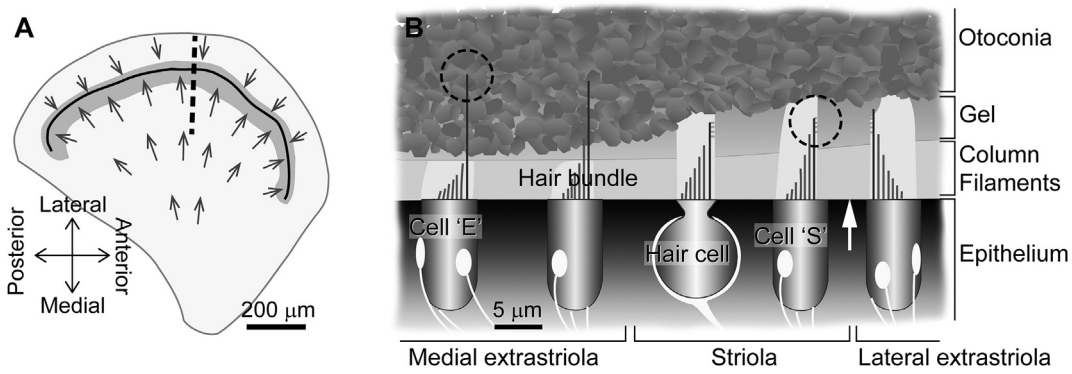

Fig. 1. Hair cells in the turtle utricle. (**A**) A schematic drawing of the epithelial surface of the turtle utricle. The arrows indicate the polarity of hair cells (the direction toward which they are most sensitive). The thick curve indicates the line of polarity reversal. The vicinity along the line of polarity reversal (indicated with the shading) is called the 'striolar' region. (**B**) Various hair cells in the turtle utricle. This cross-sectional view corresponds to the thick broken line in (A). The polarity reversal point is indicated with the white arrow in this illustration. The utricle consists of different layers. The circles with broken lines demonstrates different ways of connectivity between the hair bundles and their overlying layer (the circles with broken lines) affect the mechano-electrical transduction (MET) of the utricle. Two hair bundles (Cell E and Cell S) are modeled and simulated.

bundle of Cell S is not firmly attached to the otoconial layer. This weak coupling may not look like a good design of the mechano-transduction (MET) apparatus because the bundle's MET is activated by the deflection due to the shear displacement between the otoconial layer and the epithelial surface (the roots of the bundle).

Motivated by the anatomical feature of the turtle utricle (connectivity between the kinocilium and the otoconial layer), the possibility of fluid forcing on a striolar hair cell was examined in a previous study (Nam et al., 2005). Because little was known about what kind mechanical stimulations the utricular hair cells are subjected to under natural conditions, the implications of the study could hardly be discussed in the context of the utricle function. However, three lines of recent studies shed new light on the realistic stimulations on the utricular hair cells. Rivera et al. (2012) measured the head motion of an unconstrained turtle during feeding strike. Based on anatomical measurements, they calculated the acceleration vector components of the utricle from the head motion. Dunlap et al. (2012), Dunlap and Grant (2014) used excised turtle utricle preparations to measure the motion of the otoconial layer while the preparation stage was agitated. From these measurements, Davis and Grant (2014) derived the transfer function between the utricle acceleration and resulting otoconial layer displacement.

This study is focused on how connectivity between the hair bundle and the otoconia is related with the utricular MET. Computer models of two hair cells (Cell E and Cell S) were developed. The models feature: 1) anatomically-realistic 3-D hair bundle geometry, 2) three different stimulating conditions such as force-clamping, displacement-clamping, and viscous fluid flow, 3) up-to-date MET channel dynamics for individual channels, and 4) integrated whole utricle dynamics to simulate hair cell responses due to realistic head motions. Using these computer models, three cases were simulated: 1) Cell E displacement-clamped to the otoconial motion, 2) Cell S viscously-stimulated due to the shear flow of the sub-otoconial fluid, and 3) Cell S displacement-clamped to the otoconial motion. Taking advantage of recent data, from the head motions of the turtle, the relative motion of the otoconial layer with respect to the epithelial surface is computed. The relative motion applies either the displacement boundary condition or the viscous force boundary condition to the two representative hair cells of the turtle utricle. A realistic head motion scenario (a slow head tilt followed by a feeding strike) was simulated. How different hair cells in the turtle utricle contribute to detecting the head motion is discussed.

2. Methods

2.1. Finite element model of the hair bundle

Two modeled hair bundles represent typical bundles in the striolar region (Cell S) and the medial extrastriolar region (Cell E) of the turtle utricle (Figs. 1 and 2). The stereocilia geometrical information such as the arrangement, height and inter-ciliary spacing was obtained from microscopic images of the turtle utricle (Silber et al., 2004; Nam et al., 2006, 2007a,b). As a result, the bundle geometry is not ideally regular. The finite element (FE) model of the hair bundle is composed of two types of elements. The stereocilia are represented by beam elements which account for axial and bending deformations. The tip links running along the excitatory-inhibitory (E-I) axis connect the tips of shorter stereocilia to the shaft of taller stereocilia (Fig. 2). The horizontal connectors run along all three hexagonal axes to bind the stereocilia so that they move in unison (Cotton and Grant, 2000; 2004; Kozlov et al., 2007; Nam and Fettiplace, 2008; Karavitaki and Corey, 2010; Nam et al., 2015). The coherence of the stereocilia bundle is dependent on the stiffness of the connectors (Cotton and Grant, 2000; Nam et al., 2015). The geometrical and mechanical properties of the studied hair bundles are presented in Fig. 2 and Tables 1 and 2.

2.2. Equation of motion

The equation of motion of the hair bundle is integrated along time with a constant time step size $h = 25$ μs. This time step size is small enough to resolve the fastest kinetics of the model (the MET channels' on/off speed). The equation of motion at the $(m+1)$-th time step is described in terms of mass (**M**), damping (**C**), and stiffness (**K**) matrices, and the acceleration (**a**), velocity (**v**), displacement (**x**), and external force (**f**) vectors.

$$\mathbf{M}\mathbf{a}^{(m+1)} + \mathbf{C}\mathbf{v}^{(m+1)} + \mathbf{K}\mathbf{x}^{(m+1)} = \mathbf{f}^{(m+1)}. \quad (1)$$

The velocity and displacement at the $(m+1)$-th time step are approximated using the Newmark's method.

$$\mathbf{v}^{(m+1)} = \mathbf{v}^{(m)} + h\left\{(1-\gamma)\mathbf{a}^{(m)} + \gamma\mathbf{a}^{(m+1)}\right\}, \text{ and} \quad (2)$$

$$\mathbf{x}^{(m+1)} = \mathbf{x}^{(m)} + h\mathbf{v}^{(m)} + h^2\left\{(0.5-\beta)\mathbf{a}^{(m)} + \beta\mathbf{a}^{(m+1)}\right\}. \quad (3)$$

After reducing $\mathbf{v}^{(m+1)}$ and $\mathbf{a}^{(m+1)}$ in Eqs. (1)–(3), and introducing

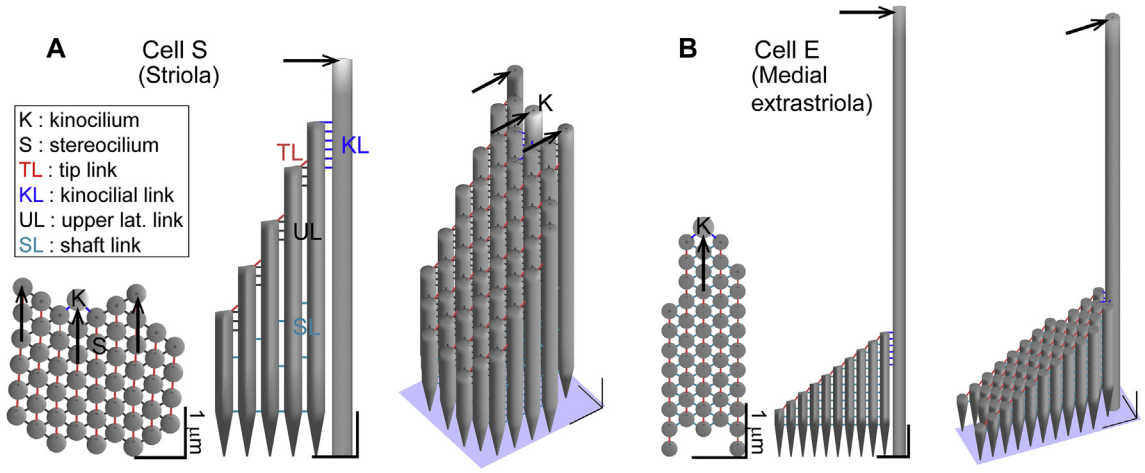

Fig. 2. Two types of hair bundles. These computer-rendered images are the finite element models of the two representative hair bundles of the turtle utricle. They are shown in three different views (planar, lateral, and 3-D views). The kinocilium and stereocilia are bound by numerous fine filaments including the tip links and different types of horizontal connectors. The arrows indicate the excitatory direction, and the assumed attachment (displacement-clamped) points to the otoconia. For Cell S, we test non-attached case, too. The scale bars indicate 1 μm. (**A**) Cell S represents a typical hair bundle in the striolar region. In the planar view, the bundle is round shaped (left). The kinocilium and the tallest row stereocilia are similar in their height. (**B**) Cell E represents a typical hair bundle in medial extrastriolar region. The bundle has more stereocilia rows along the E-I axis, and the kinocilium is much longer than the rest of the bundle.

Table 1
Model geometry (Lengths in μm).

Cell type	Cell S	Cell E
Number of stereocilia	51	48
Number of tip links	42	43
Kinocilium height	8.8	14
Stereocilia height	9.2–2.4	4–1.2
Stereocilia spacing (mean)	0.48	0.37
Kinocilium diam.	0.45	0.40
Stereocilia diam. (shaft/root)	0.4/0.04	0.3/0.04
Tip link length (mean)	0.20	0.20
Array length in E-I direction	3.2	4.1

Table 2
Mechanical and channel parameters.

Parameter	Value	Description
E_K (MPa)	9	Elastic modulus of Kinocilium
E_S (MPa)	5	Elastic modulus of stereocilia
k_{GS} (mN/m)	1	Stiffness of the gating spring
k_{UL} (mN/m)	0.5	Stiffness of the horizontal connectors
f_o (pN)	15	Setting point of resting state
k_b ($ms^{-1}\mu M^{-1}$)	0.1	Ca^{2+} binding coefficient
K_D (μM)	20	Ca^{2+} dissociation constant
k_F (ms^{-1})	2	Channel C→O rate constant
b (nm)	5	Gating swing
b_{Ca} (nm)	1	Adaptation due to Ca^{2+} binding
C_{FA} (μM)	0.1/35	[Ca^{2+}] when channel is closed/open
k_A (km/s/N)	50	Slow adaption rate
f_M (pN)	12	Stalling force of slow adaptation
k_{ES} (mN/m)	2	Stiffness of the extent spring

$\mathbf{u}^{(m+1)} = \mathbf{x}^{(m+1)} - \mathbf{x}^{(m)}$, we obtain

$$\left(\mathbf{K} + \mathbf{K}_{eff}\right)\mathbf{u}^{(m+1)} = \mathbf{f}^{(m+1)} - \mathbf{p}^{(m)} + \mathbf{C}_{eff}\mathbf{v}^{(m)} + \mathbf{M}_{eff}\mathbf{a}^{(m)} - \mathbf{K}_{eff}\mathbf{u}^{(m)}, \quad (4)$$

where $\mathbf{K}_{eff} = \mathbf{M}/(\beta h^2) + \mathbf{C}(\gamma/\beta h)$, $\mathbf{C}_{eff} = \mathbf{M}/(\beta h) + \mathbf{C}(\gamma/\beta - 1)$, and $\mathbf{M}_{eff} = \mathbf{M}/(0.5\beta - 1) + \mathbf{C}(0.5\gamma/\beta - 1)h$. The internal reaction force $\mathbf{p}^{(m)} = \mathbf{K}\mathbf{x}^{(m)}$. The coefficient values are $\beta = 0.3333$ and $\gamma = 0.5005$.

Although the mass is explicitly expressed in this formulation to be consistent with the general Newmark formulation, the inertial term is more than three orders of magnitude smaller than the damping and the stiffness terms (Nam et al., 2005). Therefore, the mass of the stereocilia hardly affects the results. The damping matrix is determined using the Rayleigh damping, $\mathbf{C} = \alpha_C\mathbf{K} + \beta_C\mathbf{M}$. With the given coefficient values of $\boldsymbol{\alpha_C} = 0.1$ μs, and $\beta_C = 0.4$ ms^{-1}, the time constant of the bundle deflection due to a step force is 0.5 and 0.7 ms for Cell S and Cell E. The flexural rigidity of the stereocilia is determined by the dimension and the elastic moduli of the stereocilia (Table 2). Those values were chosen to match experimentally measured stiffness of similar hair bundles in the turtle utricle (Spoon et al., 2011).

2.3. Displacement-clamped hair bundle

When the hair bundle is deflected by the relative motion between two stiff layers (the otoconial and the epithelial layers), the hair bundle displacement at the attachment point equals the relative motion between the two layers. That is, the hair bundle is considered to be 'displacement-clamped'. The assumed locations of displacement-clamp were indicated with the arrows in Fig. 2. To solve for given displacement instead of given force, the equation of motion needs to be reorganized so that the given displacement is on the right-hand-side of the equation. The displacement vector is divided into the given (clamped) degrees of freedom $\mathbf{u}_2$ and the remaining degrees of freedom $\mathbf{u}_1$, or

$$\mathbf{u} = \begin{pmatrix} \mathbf{u}_1 \\ \mathbf{u}_2 \end{pmatrix} \quad (5)$$

If we put $\overline{\mathbf{K}} = \mathbf{K} + \mathbf{K}_{eff}$, and $\overline{\mathbf{f}}^{(m)} = -\mathbf{p}^{(m)} + \mathbf{C}_{eff}\mathbf{v}^{(m)} + \mathbf{M}_{eff}\mathbf{a}^{(m)} - \mathbf{K}_{eff}\mathbf{u}^{(m)}$, the notation of Eq. (5) applies to these terms, such that

$$\overline{\mathbf{K}} = \begin{pmatrix} \overline{\mathbf{K}}_{11} & \overline{\mathbf{K}}_{12} \\ \overline{\mathbf{K}}_{21} & \overline{\mathbf{K}}_{22} \end{pmatrix}, \text{ and} \quad (6)$$

$$\overline{\mathbf{f}} = \begin{pmatrix} \overline{\mathbf{f}}_1 \\ \overline{\mathbf{f}}_2 \end{pmatrix}. \quad (7)$$

Using Eqs. (5)–(7), the equation to solve for the displacement-clamped condition is

$$\overline{\mathbf{u}}_1^{(m+1)} = \left(\overline{\mathbf{K}}_{11}\right)^{-1}\left(\overline{\mathbf{f}}_1^{(m)} - \overline{\mathbf{K}}_{12}\overline{\mathbf{u}}_2^{(m+1)}\right). \tag{8}$$

In our case, the term $\mathbf{u}_2$ equals the relative shear displacement between the otoconial and the epithelial layers.

2.4. Viscously-clamped deformation of hair bundle

Hair bundle deflection is small (angular displacement is less than three degrees), and the relevant fluid flow is highly viscous (Reynolds number Rn < 0.001). For these reasons, it was assumed that the fluid applies force to the bundle, but the bundle does not disturb the fluid. Instead of solving fluid dynamics explicitly, the fluid-induced force was approximated from viscous drag on a cylinder. The drag force D, on a cylindrical object caused by viscous fluid flow is determined by the mass density of fluid ρ, the relative velocity between the cylinder (stereocilium) and the fluid V, the area of the cylinder projected to the fluid flow A, the mass density of the fluid ρ, and the drag coefficient C_D.

$$D = C_D\frac{1}{2}\,\rho A|V|V. \tag{9}$$

Since each stereocilium has a long cylindrical shape, and the Reynolds number (Rn) is much less than 1, the drag coefficient C_D will be approximated by the Oseen's formulation (White, 1986).

$$C_D = 8\pi/(Rn\,\log(7.4/Rn)). \tag{10}$$

The Reynolds number is defined as $Rn = \rho Vd/\mu$, where d is the stereocilia diameter, and μ is the dynamic viscosity of the fluid. We assume the viscosity of the endolymph fluid to be the same as water (1 mPa s). The fluid drag on the extracellular links was ignored, which may have resulted in some underestimation of fluid drag.

In our simulation, the relative motion between the otoconial and the epithelial layers was considered to generate a linearly developing shear flow (Fig. 3A). At each time step, the relative velocity between the stereocilia surface and the fluid was used to compute the nodal drag force (Fig. 3C). Note that when the 'displacement-clamped' condition is considered, there is no relative velocity. That is, when the bundle is firmly attached to its overlying layer, there is no drag force due to the fluid external to the bundle.

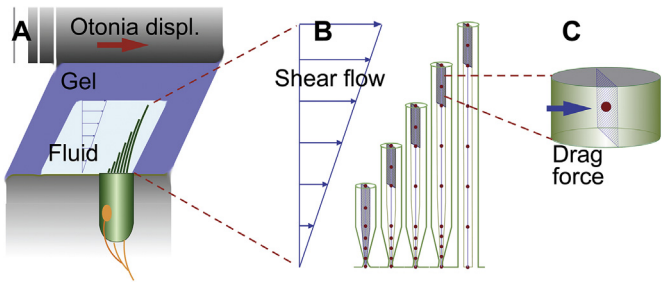

Fig. 3. Viscously-coupled hair bundle. (**A**) Due to the displacement of the otoconial layer relative to the epithelium, the compliant layer where the hair bundles stand is shear deformed. (**B**) The fluid around the hair bundle forms a shear flow. The red dots indicate the nodes of the FE model. The shaded areas indicate the projected area normal to the flow in the direction shown. (**C**) Using the relative fluid velocity to the stereocilia, and the projected area, the nodal drag force is obtained.

2.5. Mechano-electric transduction (MET)

The MET channel kinetics of the present study are similar to previous studies (Beurg et al., 2008; Nam and Fettiplace, 2008). There are two main differences. First, the rate coefficients are smaller than those in the previous study where the rodent hair cell MET was modeled. Second, the slow adaption that we neglected in the previous studies was incorporated because, unlike mammalian auditory hair cell, the slow adaption characterizes vestibular hair cells (Eatock, 2000).

The channel has two configurational states (open or closed), and five (zero to four) calcium-dependent states assuming four calcium-binding site within the channel pore. The transition between the open and closed state are determined stochastically by two rate coefficients,

$$\begin{cases} k_{CO} = k_F\,\exp(\Delta E/2k_BT) \\ k_{OC} = k_F\,\exp(-\Delta E/2k_BT) \end{cases}, \tag{11}$$

where the constant k_BT is 4.1 × 10^{-21} J, and the constant k_F determines the MET channel activation speed.

The calcium-binding and unbinding rates are defined as,

$$\begin{cases} k_{Ca}^{+} = k_b C_{FA} \\ k_{Ca}^{-} = k_b K_D \end{cases}. \tag{12}$$

In these equations, k_b is calcium binding coefficient, C_{FA} is calcium concentration at the binding site, and K_D is the dissociation constant. The energy difference between open and closed states ΔE is defined as a function of the tip link tension f_{GS}.

$$\Delta E = b\,(f_{GS} - f_0). \tag{13}$$

Here, b is the gating swing, and f_0 is a constant used to set the resting open probability. The tip link tension varies as its unstrained length, l_{TL}^0, changes due to channel opening/closing, calcium finding and slow adaptation. In the model, l_{TL}^0 is increased by b when the MT channel opens, by b_{Ca} when the channel binds a calcium ion, and by x_A due to slow adaption, or

$$l_{TL,new}^0 = l_{TL}^0 + n_O\,b - n_{Ca}b_{Ca} + x_A. \tag{14}$$

The coefficient n_O is 0 when the channel is closed, and 1 when open. n_{Ca} is the number of calcium ions bound to the channel, which is between 0 and 4. Any variation in the unstrained length changes the stiffness $\mathbf{K}$ and the internal force $\mathbf{p}$ in Eq. (4). This change affects the internal force equilibrium of the FE model to adjust the tension, f_{GS}. The slow adaptation is governed by a first order kinetics of

$$\dot{x}_A = k_A(f_{GS} - f_M - k_{ES}x_A), \tag{15}$$

where f_M and k_{ES} are the constants determining the adaptation motor's stalling force, and the extent of adaptation (Shepherd and Corey, 1994), respectively. The upper dot denotes the time derivative.

In this study, the tip link represents not only the extracellular filaments, but includes all the components in series with the extracellular filaments between the stereocilia actin cores. The stiffness of the tip link represents the stiffness of yet-putative gating spring, k_{GS}. Therefore, the tension in the tip link, f_{GS}, equals the tension experienced by the MET channel.

2.6. Utricle dynamics

The utricle dynamics was adopted from Dunlap and Grant

(2014) and Grant and Curthoys (2017). In the studies, the authors presented the transfer function between the head acceleration (a_{Head}) and the shear displacement of the otoconial layer with respect to the epithelium (x_{OL}) of the turtle utricle. The equation of motion along the medial-lateral axis is

$$\ddot{x}_{OL} + 2\zeta\omega_n\dot{x}_{OL} + \omega_n^2 x_{OL} = -B(a_{Head} - g_x). \quad (16)$$

After Dunlap et al.'s measurement (Dunlap and Grant, 2014), the damping coefficient and the undamped natural frequency were $\zeta = 0.5$ and $\omega_n = 2420$ rad/s (385 Hz), respectively. The constant B is determined by the ratio of mass densities between the otoconial layer and the fluid, and the value was estimated to be $B = 0.578$. The last term g_x represents the component of gravitational acceleration along the considered axis.

When the tip of hair bundle is firmly attached to the otoconia, the motion of the otoconial layer with respect to the epithelium equals the hair bundle tip displacement, or $x_{OL} = x_{HB}$. The hair bundle tip displacement x_{HB} equals the term u_2 in Eq. (8). When the hair bundle is not attached to the otoconia, its motion is considered viscously coupled to the otoconia through the endolymph fluid. Hereafter, the two stimulating conditions are called the displacement-clamped (X-clamped), and viscously-coupled (V-clamped) condition. Also, x_{OL} and $\dot{x}_{OL}$ are loosely called as the otoconial displacement and velocity.

According to these values and definition, when the head rolls 45°, the X-clamped hair bundle deflects as large as 0.7 μm. When the head receives a step stimulation at the level of 1 g (9.8 m/s^2), the peak fluid velocity that the hair bundle is subjected to is 1.3 mm/s.

2.7. Computation

The computer program for this study is written in Matlab (ver. 9.0, Mathworks, Natick, MA). The problem size of the combined system was about 2500 and 3600 degrees-of-freedom for Cell E and Cell S. When run on an IBM PC (Intel i7-6700 processor, 3.4 GHz, 16 GB RAM), it takes about 1 min to solve for the time span of 100 ms. The simulation code is available through the research webpage of the corresponding author.

3. Results

All results but Fig. 4 are hair cell MET responses to given head accelerations (a_{Head} in Eq. (16)). In Fig. 4, the MET transfer functions of individual hair cells are presented—the relationship between the normalized MET current and the hair bundle displacement (i_{MET} versus x_{HB}). The MET responses of the utricle, the relationship between i_{MET} and a_{Head}, are presented in Figs. 5–7. In Fig. 8, the utricular MET due to realistic head motion of a turtle is simulated. For all results (but Fig. 4), three cases are presented: X-clamped Cell E, V-clamped Cell S, and X-clamped Cell S.

3.1. MET responses of the two hair bundles

The MET responses of the modeled two cells are comparable (Fig. 4A and B), simply because the same set of MET properties were used for both cells. Note that this study is focused on the difference in hair bundle mechanics, because it is not known whether the MET channels in different types of hair cells are different. Physiologically observed characteristics of MET current were reproduced with the present model. First, the MET current decays after a peak for a sustained stimulation (Eatock et al., 1987; Holt et al., 1998). Second, the MET current have fast and slow adaptation components (Ricci and Fettiplace, 1998). In this study, the respective time constants were 0.8 and 8 ms. Similar to experimental observations, the fast component is more prominent at small stimulation levels (Wu et al., 1999; Vollrath and Eatock, 2003). Finally, the action of MET channels affects bundle mechanics (Howard and Hudspeth, 1988; Holt and Corey, 2000). For example, an event of channel opening/closing results in positive/negative bundle displacement. The slow adaptation causes creeping bundle displacement after the peak.

There exists a clear difference in the MET characteristics of Cell E and Cell S, due to their different geometry. The Cell E hair bundle is

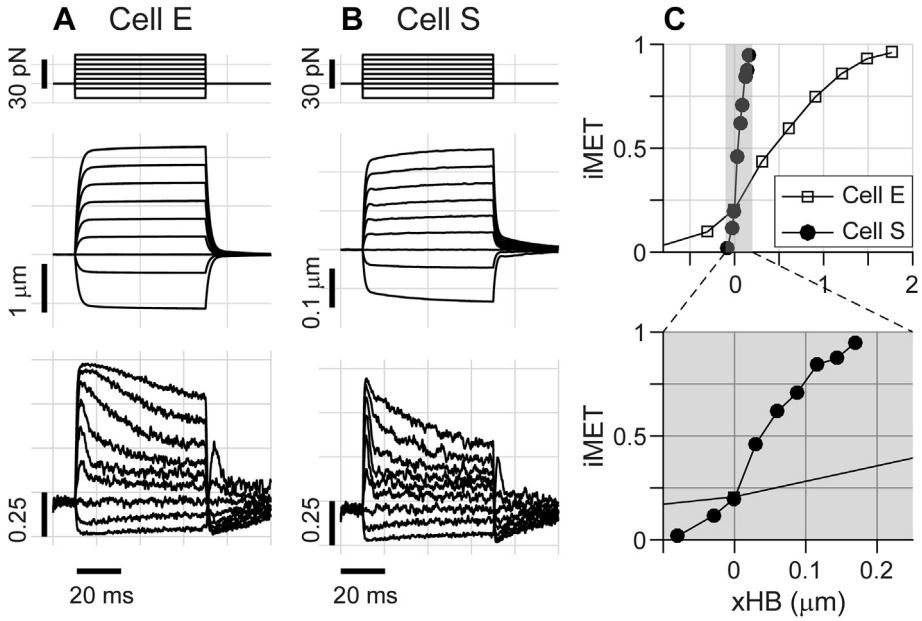

Fig. 4. MET of two hair bundles. A series of step forces were applied to the tips of the Cell E and Cell S hair bundles. (**A**, **B**) Cell E and Cell S responses. From the top to the bottom, applied forces, resulting bundle tip displacements (x_{HB}), and normalized MET currents (i_{MET}). The i_{MET} curves look noisy even after averaging ten trials, because of stochastic MET channel responses. (**C**) Current-displacement relationships of the two cells. To present the different operating ranges better, the same curves were presented twice for different x_{HB} ranges.

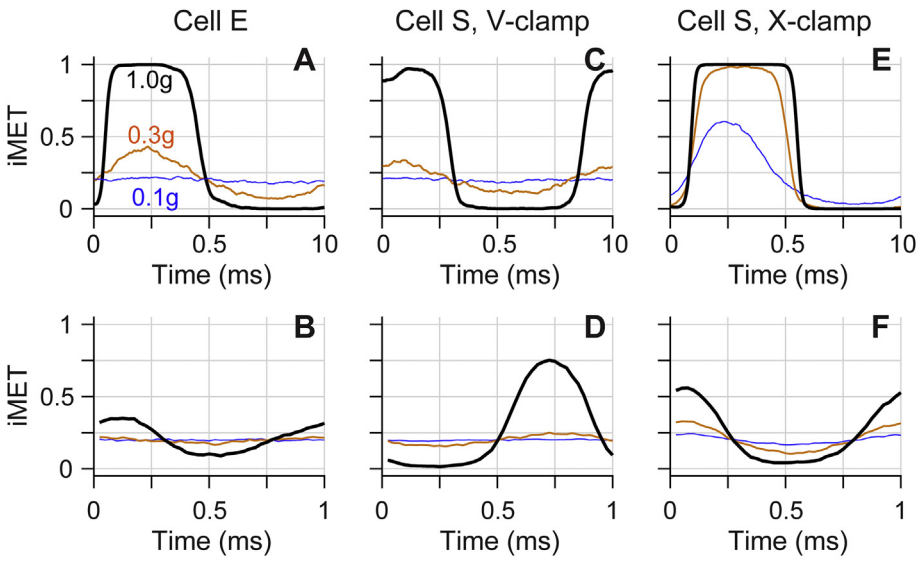

Fig. 5. Responses to sinusoidal stimulations. The two hair cells' MET responses over a cycle are plotted, when the turtle head was subjected to pure tone stimulations. Top panels and bottom panels correspond to 100 Hz and 1000 Hz head oscillations, respectively. Each panel presents the responses to three different stimulation levels (1, 0.3 and 0.1 times the gravitational acceleration). (**A**, **B**) X-clamped Cell E. (**C**, **D**) V-clamped Cell S. (**E**, **F**) X-clamped Cell S.

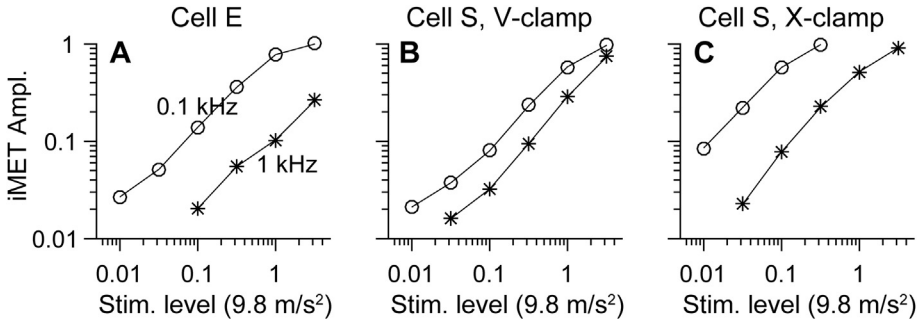

Fig. 6. Response to different stimulation levels. The simulations shown in Fig. 5 were repeated for a wide range of stimulus levels. The peak-to-peak amplitudes of i_{MET} are plotted versus the stimulus level. (**A**) X-clamped Cell E. (**B**) V-clamped Cell S. (**C**) X-clamped Cell S.

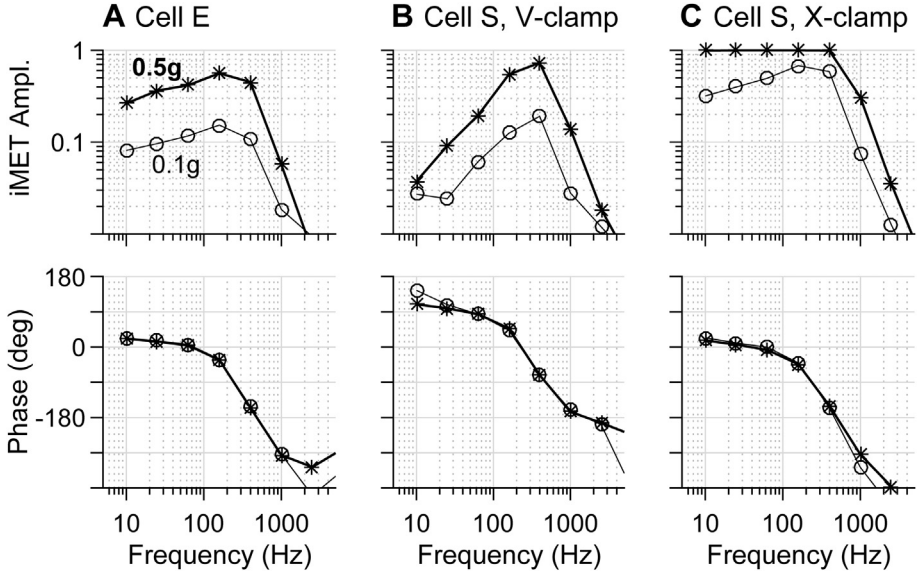

Fig. 7. Transfer function of the utricle. The simulations shown in Fig. 5 were repeated for a wide range of stimulus frequencies. The amplitude and phase of i_{MET} when the turtle head is subjected to different vibration frequencies. (**A**) X-clamped Cell E. (**B**) V-clamped Cell S. (**C**) X-clamped Cell S.

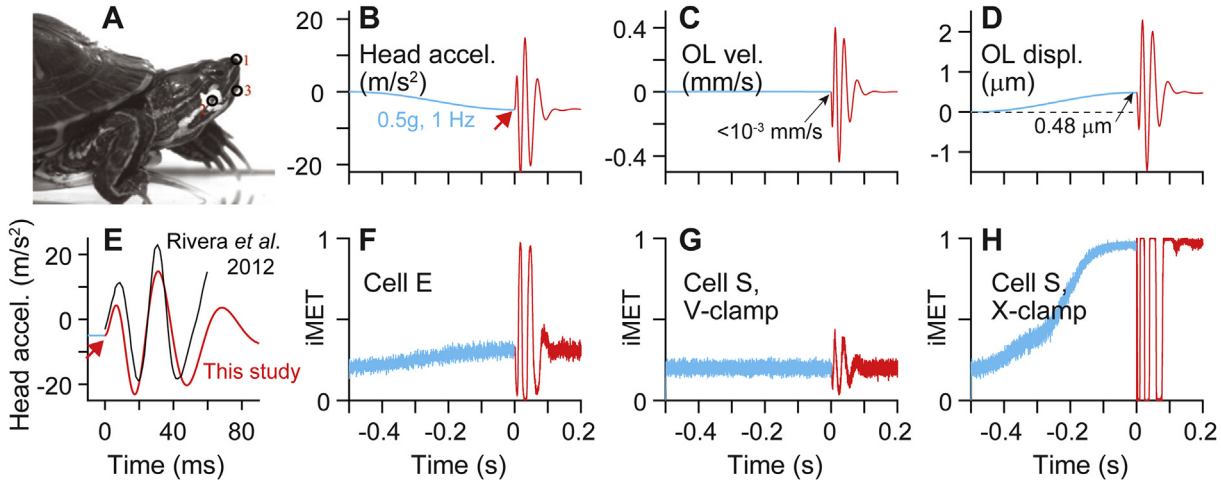

Fig. 8. MET responses of natural stimulation. (**A**) Rivera et al. (2012) measured natural motion of the turtle head during a feeding strike. Image courtesy of Dr. M. Rowe. (**B**) A hypothetical yet realistic head acceleration scenario. The head tilts slowly (blue curve, 0.5 g at 1 Hz). Then at $t = 0$ s, the head moves quickly for a feeding strike. (**C**) Resultant velocity of the otoconial layer relative to the head (epithelium). Note that there is negligible velocity during the slow tilt. (**D**) Resultant displacement of the otoconial layer relative to the head (epithelium). Note that there is considerable displacement (0.48 μm) due to the tilt. (**E**) Comparison between our assumed head motion and the measured motion. (**F**–**H**) MET responses of the hair cells to the realistic head motion: X-clamped Cell E, V-clamped Cell S, X-clamped Cell S.

about one order of magnitude more compliant than the Cell S hair bundle. The stiffness values of the modeled hair bundles (14 μN/m for the Cell E and 140 μN/m for Cell S) are comparable to experimental measurements of similar hair bundles (Spoon and Grant, 2011; Spoon et al., 2011). As a result, the MET operating ranges, the bundle displacement span to activate between 10 and 90 percent of MET current, of the two cells are different—1.7 μm for Cell E versus 0.18 μm for Cell S (Fig. 4C). This difference has its consequence to the function of the turtle utricle, because the hair bundles in the turtle utricle can be subjected to more than 1 μm displacement (Dunlap et al., 2012), which will saturate the MET of Cell S.

3.2. Hair cell MET response to sinusoidal head motion

Using the utricle dynamics identified by Dunlap and Grant (Eq. (16), (Dunlap and Grant, 2014)), the motion of the otoconial layer due to sinusoidal head acceleration was obtained. It was assumed that the otoconial motion relative to the skull (or the epithelium) stimulates the utricular hair bundles in two different ways. First, the hair bundles are tightly coupled to the otoconia so that they are displacement-clamped (X-clamp condition). Second, the hair bundles have little elastic attachment to the otoconia so that they are viscously-coupled (V-clamp condition).

In Fig. 5, the turtle head oscillated at two different frequencies (100 and 1000 Hz) and with three different amplitudes (0.1, 0.3, and 1.0 times the gravitational acceleration level). Because 100 Hz is about two octaves below the characteristic frequency of the utricle (385 Hz according to (Dunlap and Grant, 2014)), and an octave slower than the hair cell's adaptation, that stimulation speed may be considered quasi-static. The amplitudes of the otoconial displacement were 1.0 and 0.16 μm per 1 g for 0.1 and 1 kHz stimulation, respectively. The corresponding velocity amplitudes were 0.63 and 0.96 mm/s per 1 g. The MET current responses over a stimulation cycle are sinusoidal at small stimulation levels, but the curve shapes deviate from pure sinusoid as the MET current saturates at large stimulation levels (black curves of 1.0 g-level in Fig. 5). As the otoconial displacement is low-pass filtered at approximately 400 Hz, i_{MET} of the X-clamped hair bundles was decreased at 1000 Hz as compared to the 100 Hz case. As the otoconial velocity peaks near 400 Hz, i_{MET} of the V-clamped Cell S remains significant at 1 kHz (Fig. 5D). If Cell S is X-clamped, however, the cell is prone to saturate even for modest head tilt (Fig. 5E). For example, the 0.3 g stimulation, equivalent to the 17.5 degrees of head tilt (*i.e.*, $\sin(17.5°) = 0.3$), saturated the cell.

3.3. The operating range of the utricle (in g-level)

The two hair cells were subjected to different levels of head acceleration between 0.01 and 3 times the g-level at two different oscillating frequencies (100 and 1000 Hz). In Fig. 6, peak-to-peak i_{MET} amplitudes were plotted versus the stimulation (head acceleration) level. These plots suggest the operating range of the turtle utricle—the span of g-level to modulate the i_{MET} amplitude between 0.1 and 0.9. If the i_{MET} amplitude is too small (<0.1), the stimulation will be difficult to detect. If the i_{MET} amplitude is too large (>0.9), the stimulation will saturate (over-stimulates) the hair cells.

The operating range of the turtle utricle can be estimated from Fig. 6. For slow stimulations (<100 Hz), The operating range of the X-clamped Cell E was between 0.06 and 2.0 times the g-level. At 1000 Hz, it took nearly 1.0 g for Cell E to excite $i_{MET} > 0.1$. The V-clamped Cell S performed better at high frequency as compared to Cell E. Its operating range at 1000 Hz was between 0.3 g and 4 g, and at 100 Hz, it was between 0.1 g and 2.6 g. That is, the V-clamped Cell S may operate well over a wide g-range for frequency range between 100 and 1000 Hz. In contrast, when Cell S is X-clamped, it is easily saturated, especially at low frequencies. For example, at 100 Hz, as low stimulation as 0.26 g consumes 90 percent of the i_{MET} capacity. This g-level corresponds to 15 degrees of head tilt.

3.4. The transfer function of the turtle utricle's MET

The simulations shown in Fig. 5 were repeated for different frequencies between 10 and 4000 Hz. The results of two different stimulation levels, 0.1 g and 0.5 g, are presented in Fig. 7. Cell E is most sensitive near the resonant frequency of the utricle (385 Hz), and it remains sensitive below the frequency (Fig. 7A). This low-pass-filter characteristic is consistent with the utricle mechanics (Grant and Curthoys, 2017). When V-clamped, Cell S was sensitive around the utricle's characteristic frequency. However, at low (<50 Hz) or high frequencies (>1000 Hz), the V-clamped Cell S was

not as sensitive (i_{MET} amplitude < 0.1 at 0.5 g, Fig. 7B). This band-pass-filter characteristic is primarily due to the utricle mechanics. The MET channel also contributes to this filtering, but its effect was modest in this study. With the given MET channel properties, the MET channel behaves like a band-pass filter (cutoff frequencies at 200 Hz due to adaptation, and at 2.4 kHz due to channel's onset speed). Consistent with its viscous coupling mechanism, i_{MET} of the V-clamped case leads the phase of the X-clamped case by about 90° (Fig. 7B lower panel). When X-clamped, Cell S was saturated for the stimulation level of 0.5 g at < 500 Hz. That is, if Cell S is X-clamped, it may saturate even at modest head tilt (0.5 g-level corresponds to 30 degrees of tilt).

The phase difference of 90° between the two types of mechanical stimulation may provide an opportunity to compare with physiological measurements. Indeed, there were studies regarding the phase relationship between vestibular neural responses and mechanical stimulations (e.g., (Goldberg et al., 1990a,b; Brichta and Goldberg, 2000; Holt et al., 2006; Songer and Eatock, 2013)). A fraction of measured phase difference was ascribed to otoconial mechanics. However, because recordings were mostly measured at < 10 Hz, it is difficult to directly compare with the phase difference in this study. Experiments with high frequency (>100 Hz) stimulations such as the vestibular evoked myogenic potential measurements (Curthoys et al., 2006; Curthoys et al., 2012; Forbes et al., 2013; Curthoys et al., 2016) may be more comparable to the simulation protocol of this study.

3.5. Simulating the utricle MET under a realistic head motion scenario

A realistic scenario of turtle head motion was simulated (Fig. 8). In the scenario, the head was subjected to a 0.5 g acceleration over 0.5 ms (1 Hz). This is to consider the condition of quasi-static head tilt of 30°. This static head tilt is followed by a quick head motion during feeding strike. Rivera et al. used fast video imaging at two different views to measure 3-D head motion during an underwater feeding strike of a turtle (Rivera et al., 2012). The utricle accelerations in its three orthogonal axes was computed from the head motion. For the computation, they used the geometric information of the utricle within the skull obtained from micro-CT images. According to their measurement, the peak amplitude of acceleration was about 20 m/s^2, and the primary frequency was about 50 Hz (Fig. 8D).

In Fig. 8, the slow tilting stage and the fast striking stage are indicated with different colors. The assumed head motion is shown in panel B. Using the utricle transfer function of Eq. (16), the otoconial motion in the utricle was computed (panels C and D). The otoconial velocity is negligible during the tilting stage (<1 μm/s), but it reaches up to 0.4 mm/s during the striking motion. The otoconial displacement reaches 0.48 μm due to the quasi-static tilt, and the layer is further displaced up to 2.3 μm during the feeding-strike.

The simulation of realistic motion suggests that the two types of hair cells may play different role in a turtle's perception of head orientation and motion. During the quasi-static tilting period, Cell E encoded the time course of tilt without being saturated, while Cell S was either unresponsive or saturated depending on its assumed clamping mode (blue curves in panels F, G and H). During the feeding-strike motion, both Cell E and the X-clamped Cell S were saturated, but Cell S responded without saturation.

4. Discussion

4.1. An operating principle of the turtle utricle

Due to its long kinocilium, Cell E is deeply embedded into the otoconial layer. If Cell S is also firmly attached to the otoconial layer, it will saturate even for a modest head tilt. For example, quasi-static motion with the stimulation amplitude level of 0.3 g that is equivalent to 17 degrees of head tilt saturated the X-clamped Cell S (Fig. 5E). When the utricle consists of a combination of different types of hair cells such as the X-clamped Cell E and the V-clamped Cell S, it can encode a wide range of head acceleration (0.02 g and 3 g) over a wide range of frequency (DC to 3 kHz, Figs. 6 and 7). When a realistic head motion was simulated (a 30 degrees of head tilt followed by a feeding strike), the X-clamped Cell E encoded the head tilt faithfully (without being nonresponsive or being saturated), but saturated during the feeding strike.

Different stimulation scenarios were summarized in Fig. 9. To be comprehensive, the viscously-coupled condition of Cell E was presented as well (although such condition may not exist in the natural turtle utricle). When both cells types are V-clamped to the otoconial layer, the utricle will not be able to detect low frequency motion (i_{MET} amplitude < 0.04 for < 10 Hz at the level of 0.5 g). In contrast, when all utricular hair cells are X-clamped, it is difficult to detect a quick head motion. By incorporating two mechanical stimulation modalities (rigid coupling and viscous coupling between the hair bundles and the otoconia), the turtle utricle can perform a dual sensor: as a static head orientation sensor, and a motion detector over a wide operating range both in stimulating amplitude and in frequency. We believe that this mechanism may apply to the utricles of other species.

4.2. Further considerations

The same MET properties for the different types of hair cells were used in this study (Fig. 4 and Table 2). It was assumed so because the MET properties are not well known for different types of the turtle utricular hair cells, and because this study is focused on the mechanical connectivity between the hair bundles and the otoconial layer. That being said, it is presumable that different types of hair cells have different MET properties. If Cell E has slower and smaller extent of adaptation, it may enhance its sensitivity as a position sensor at the sacrifice of operating range. Cell S can have adaptation and channel activation properties so that it can pick up vibrations at certain frequency range selectively.

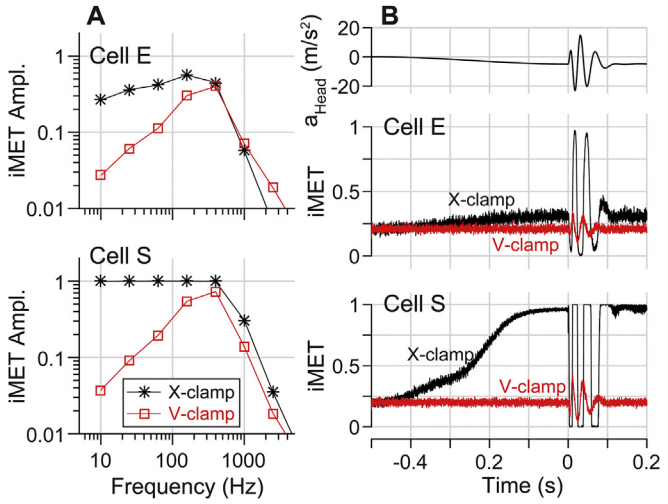

Fig. 9. Comparison between different stimulation conditions. (**A**) The turtle head is subjected to sinusoidal head motion with the amplitude of 0.5 g. The MET responses of Cell E (top) and Cell S (bottom) when X-clamped or V-clamped. (**B**) A replot of Fig. 8 (natural stimulation). Four cases are compared: Cell E and Cell S; X-clamped and V-clamped.

This study is focused on how Cell E and Cell S are coupled to the otoconial layer. For the X-clamped case, exactly where the bundle is clamped affects the MET sensitivity. For Cell S, when X-clamped, the three ciliary tips (arrows in Fig. 2A) were clamped to the otoconial layer. Had only the kinocilium tip been clamped (instead of the three tips), Cell S responds less sensitively—the MET operating range (the hair bundle displacement span to change i_{MET} between 0.1 and 0.9) increases to 0.24 μm as compared to 0.16 μm in the standard case shown in Fig. 4. Had more stereocilia tips in the tallest row of Cell S been clamped, the sensitively hardly changes (MET operating range remains at 0.16 μm). This variation of sensitivity due to the distribution of stimulation also depends on the coupling rigidity between stereocilia determined by the numerous horizontal connectors (Nam et al., 2015). For Cell E, it is clear that only the kinocilium is embedded into the otoconial layer, but at which elevation it can be considered to be clamped is unclear. This study assumed that the tip of kinocilium (at the height of 14 μm) is X-clamped with the otoconial layer. If the mid-point of the embedded part of kinocilium (at the height of 10 μm) is clamped instead, Cell E responds more sensitively—the MET operating range decreases to 0.65 μm as compared to 1.6 μm in the standard case shown in Fig. 4.

Acknowledgements

The author gratefully acknowledges the help of Drs. Wally Grant, John R. Cotton, and Ellengene Peterson at earlier stage of this work. This research is supported by NIH NIDCD R01 DC014685, and NSF CMMI-1661413.

Appendix A. Supplementary data

Supplementary data related to this article can be found at https://doi.org/10.1016/j.heares.2017.09.015.

References

Beurg, M., Nam, J.H., Crawford, A., Fettiplace, R., 2008. The actions of calcium on hair bundle mechanics in mammalian cochlear hair cells. Biophys. J. 94 (7), 2639–2653.
Brichta, A.M., Goldberg, J.M., 2000. Morphological identification of physiologically characterized afferents innervating the turtle posterior crista. J. Neurophysiol. 83 (3), 1202–1223.
Cotton, J., Grant, W., 2004. Computational models of hair cell bundle mechanics: II. Simplified bundle models. Hear Res. 197 (1–2), 105–111.
Cotton, J.R., Grant, J.W., 2000. A finite element method for mechanical response of hair cell ciliary bundles. J. Biomech. Eng. 122 (1), 44–50.
Curthoys, I.S., Kim, J., McPhedran, S.K., Camp, A.J., 2006. Bone conducted vibration selectively activates irregular primary otolithic vestibular neurons in the Guinea pig. Exp. Brain Res. 175 (2), 256–267.
Curthoys, I.S., Vulovic, V., Burgess, A.M., Sokolic, L., Goonetilleke, S.C., 2016. The response of Guinea pig primary utricular and saccular irregular neurons to bone-conducted vibration (BCV) and air-conducted sound (ACS). Hear Res. 331, 131–143.
Curthoys, I.S., Vulovic, V., Sokolic, L., Pogson, J., Burgess, A.M., 2012. Irregular primary otolith afferents from the Guinea pig utricular and saccular maculae respond to both bone conducted vibration and to air conducted sound. Brain Res. Bull. 89 (1–2), 16–21.
Davis, J.L., Grant, J.W., 2014. Turtle utricle dynamic behavior using a combined anatomically accurate model and experimentally measured hair bundle stiffness. Hear Res. 318, 37–44.
Dunlap, M.D., Grant, J.W., 2014. Experimental measurement of utricle system dynamic response to inertial stimulus. J. Assoc. Res. Otolaryngol. 15 (4), 511–528.
Dunlap, M.D., Spoon, C.E., Grant, J.W., 2012. Experimental measurement of utricle dynamic response. J. Vestib. Res. 22 (2), 57–68.
Eatock, R.A., 2000. Adaptation in hair cells. Annu. Rev. Neurosci. 23, 285–314.
Eatock, R.A., Corey, D.P., Hudspeth, A.J., 1987. Adaptation of mechanoelectrical transduction in hair cells of the bullfrog's sacculus. J. Neurosci. 7 (9), 2821–2836.
Fernandez, C., Goldberg, J.M., Baird, R.A., 1990. The vestibular nerve of the chinchilla. III. Peripheral innervation patterns in the utricular macula. J. Neurophysiol. 63 (4), 767–780.
Forbes, P.A., Dakin, C.J., Vardy, A.N., Happee, R., Siegmund, G.P., Schouten, A.C., Blouin, J.S., 2013. Frequency response of vestibular reflexes in neck, back, and lower limb muscles. J. Neurophysiol. 110 (8), 1869–1881.
Goldberg, J.M., Desmadryl, G., Baird, R.A., Fernandez, C., 1990a. The vestibular nerve of the chinchilla. IV. Discharge properties of utricular afferents. J. Neurophysiol. 63 (4), 781–790.
Goldberg, J.M., Desmadryl, G., Baird, R.A., Fernandez, C., 1990b. The vestibular nerve of the chinchilla. V. Relation between afferent discharge properties and peripheral innervation patterns in the utricular macula. J. Neurophysiol. 63 (4), 791–804.
Grant, J.W., Curthoys, I.S., 2017. Otoliths - accelerometer and seismometer; implications in vestibular evoked myogenic potential (VEMP). Hear Res. (To appear).
Holt, J.C., Xue, J.T., Brichta, A.M., Goldberg, J.M., 2006. Transmission between type II hair cells and bouton afferents in the turtle posterior crista. J. Neurophysiol. 95 (1), 428–452.
Holt, J.R., Corey, D.P., 2000. Two mechanisms for transducer adaptation in vertebrate hair cells. Proc. Natl. Acad. Sci. U. S. A. 97 (22), 11730–11735.
Holt, J.R., Corey, D.P., Eatock, R.A., 1998. Mechanoelectrical transduction and adaptation in hair gels of the mouse utricle, a low-frequency vestibular organ (vol. 17, pg 8739, 1997). J. Neurosci. 18 (16). Cp4-Cp4.
Howard, J., Hudspeth, A.J., 1988. Compliance of the hair bundle associated with gating of mechanoelectrical transduction channels in the bullfrog's saccular hair cell. Neuron 1 (3), 189–199.
Hudspeth, A.J., Corey, D.P., 1977. Sensitivity, polarity, and conductance change in the response of vertebrate hair cells to controlled mechanical stimuli. Proc. Natl. Acad. Sci. U. S. A. 74 (6), 2407–2411.
Karavitaki, K.D., Corey, D.P., 2010. Sliding adhesion confers coherent motion to hair cell stereocilia and parallel gating to transduction channels. J. Neurosci. 30 (27), 9051–9063.
Kozlov, A.S., Risler, T., Hudspeth, A.J., 2007. Coherent motion of stereocilia assures the concerted gating of hair-cell transduction channels. Nat. Neurosci. 10 (1), 87–92.
Li, A., Xue, J., Peterson, E.H., 2008. Architecture of the mouse utricle: macular organization and hair bundle heights. J. Neurophysiol. 99 (2), 718–733.
Nam, J.H., Cotton, J.R., Grant, J.W., 2005. Effect of fluid forcing on vestibular hair bundles. J. Vestib. Res. 15 (5–6), 263–278.
Nam, J.H., Cotton, J.R., Grant, W., 2007a. A virtual hair cell, I: addition of gating spring theory into a 3-D bundle mechanical model. Biophys. J. 92 (6), 1918–1928.
Nam, J.H., Cotton, J.R., Grant, W., 2007b. A virtual hair cell, II: evaluation of mechanoelectric transduction parameters. Biophys. J. 92 (6), 1929–1937.
Nam, J.H., Cotton, J.R., Peterson, E.H., Grant, W., 2006. Mechanical properties and consequences of stereocilia and extracellular links in vestibular hair bundles. Biophys. J. 90 (8), 2786–2795.
Nam, J.H., Fettiplace, R., 2008. Theoretical conditions for high-frequency hair bundle oscillations in auditory hair cells. Biophys. J. 95 (10), 4948–4962.
Nam, J.H., Peng, A.W., Ricci, A.J., 2015. Underestimated sensitivity of mammalian cochlear hair cells due to splay between stereociliary columns. Biophys. J. 108 (11), 2633–2647.
Rabbitt, R.D., Damiano, E.R., Grant, J.W., 2004. Biomechanics of the semicircular canals and otolith organs. In: Highstein, S.M., Fay, R.R., Popper, A.N. (Eds.), The Vestibular System. Springer, New York, pp. 153–201.
Ricci, A.J., Fettiplace, R., 1998. Calcium permeation of the turtle hair cell mechanotransducer channel and its relation to the composition of endolymph. J. Physiol. 506 (Pt 1), 159–173.
Rivera, A.R., Davis, J., Grant, W., Blob, R.W., Peterson, E., Neiman, A.B., Rowe, M., 2012. Quantifying utricular stimulation during natural behavior. J. Exp. Zool. A Ecol. Genet. Physiol. 317 (8), 467–480.
Shepherd, G.M., Corey, D.P., 1994. The extent of adaptation in bullfrog saccular hair cells. J. Neurosci. 14 (10), 6217–6229.
Silber, J., Cotton, J., Nam, J.H., Peterson, E.H., Grant, W., 2004. Computational models of hair cell bundle mechanics: III. 3-D utricular bundles. Hear Res. 197 (1–2), 112–130.
Songer, J.E., Eatock, R.A., 2013. Tuning and timing in mammalian type I hair cells and calyceal synapses. J. Neurosci. 33 (8), 3706–3724.
Spoon, C., Grant, W., 2011. Biomechanics of hair cell kinocilia: experimental measurement of kinocilium shaft stiffness and base rotational stiffness with Euler-Bernoulli and Timoshenko beam analysis. J. Exp. Biol. 214 (Pt 5), 862–870.
Spoon, C., Moravec, W.J., Rowe, M.H., Grant, J.W., Peterson, E.H., 2011. Steady-state stiffness of utricular hair cells depends on macular location and hair bundle structure. J. Neurophysiol. 106 (6), 2950–2963.
Vollrath, M.A., Eatock, R.A., 2003. Time course and extent of mechanotransducer adaptation in mouse utricular hair cells: comparison with frog saccular hair cells. J. Neurophysiol. 90 (4), 2676–2689.
White, F.M., 1986. Fluid Mechanics. McGraw-Hill, New York.
Wu, Y.C., Ricci, A.J., Fettiplace, R., 1999. Two components of transducer adaptation in auditory hair cells. J. Neurophysiol. 82 (5), 2171–2181.
Xue, J., Peterson, E.H., 2006. Hair bundle heights in the utricle: differences between macular locations and hair cell types. J. Neurophysiol. 95 (1), 171–186.